HHS Public Access

Author manuscript

Exp Eye Res. Author manuscript; available in PMC 2017 July 13.

Published in final edited form as:

Exp Eye Res. 2015 September ; 138: 126–133. doi:10.1016/j.exer.2015.05.016.

Deficiency of CC chemokine ligand 2 and decay-accelerating factor causes retinal degeneration in mice

Minzhong Yu[a,b,*], **Kai Kang**[a], **Ping Bu**[c], **Brent A. Bell**[a], **Charles Kaul**[a], **James B. Qiao**[c], **Gwen Sturgill-Short**[e], **Xiaoshan Yu**[a], **Matthew J. Tarchick**[a,e], **Craig Beight**[a], **Sarah X. Zhang**[d], and **Neal S. Peachey**[a,b,e]

[a]Department of Ophthalmic Research, Cole Eye Institute, Cleveland Clinic Foundation, Cleveland, OH, USA

[b]Department of Ophthalmology, Cleveland Clinic Lerner College of Medicine of Case Western Reserve University, Cleveland, OH, USA

[c]Department of Ophthalmology, Loyola University Chicago, Maywood, IL, USA

[d]Departments of Ophthalmology and Biochemistry, SUNY-Buffalo and SUNY Eye Institute, Buffalo, NY, USA

[e]Research Service, Louis Stokes Cleveland Veterans Affairs Medical Center, Cleveland, OH, USA

Abstract

CC chemokine ligand 2 (CCL2) recruits macrophages to reduce inflammatory responses. Decay-accelerating factor (DAF) is a membrane regulator of the classical and alternative pathways of complement activation. In view of the link between complement genes and retinal diseases, we evaluated the retinal phenotype of C57BL/6J mice and mice lacking *Ccl2* and/or *Daf1* at 12 months of age, using scanning laser ophthalmoscopic imaging, electroretinography (ERG), histology, immunohistochemistry, and terminal deoxynucleotidyl transferase dUTP nick end labeling (TUNEL) analysis. In comparison to C57BL/6J mice, mutant mice had an increased number of autofluorescent foci, with the greatest number in the $Ccl2^{-/-}/Daf1^{-/-}$ retina. ERG amplitudes in $Ccl2^{-/-}/Daf1^{-/-}$, $Ccl2^{-/-}$ and $Daf1^{-/-}$ mice were reduced, with the greatest reduction in $Ccl2^{-/-}/Daf1^{-/-}$ mice. TUNEL-positive cells were not seen in C57BL/6J retina, but were prevalent in the outer and inner nuclear layers of $Ccl2^{-/-}Daf1^{-/-}$ mice and were present at reduced density in $Ccl2^{-/-}$ or $Daf1^{-/-}$ mice. Cell loss was most pronounced in the outer and inner nuclear layers of $Ccl2^{-/-}/Daf1^{-/-}$ mice. The levels of the endoplasmic reticulum chaperone GPR78 and transcription factor ATF4 were significantly increased in the $Ccl2^{-/-}/Daf1^{-/-}$ retina. In comparison to the C57BL/6J retina, the phosphorylation of NF-κB p65, p38, ERK and JNK was significantly upregulated while SIRT1 was significantly downregulated in the $Ccl2^{-/-}/Daf1^{-/-}$ retina. Our results suggest that loss of *Ccl2* and *Daf1* causes retinal neuronal death and degeneration which is related to increased endoplasmic reticulum stress, oxidative stress and inflammation.

[*]Corresponding author. Cole Eye Institute, Cleveland Clinic Foundation, 9500 Euclid Ave, Cleveland, OH 44195, USA. yum@ccf.org (M. Yu).

Keywords

Retinal degeneration; CC chemokine ligand 2; Decay accelerating factor; Endoplasmic reticulum stress; Oxidative stress; Apoptosis

1. Introduction

Monocytes, macrophages and microglia (MMM) play important roles in the retina by clearing cellular debris. During inflammation, CC chemokine ligand 2 (CCL2) is upregulated (Deshmane et al., 2009), stimulating the migration and infiltration of MMM cells along a chemical gradient to sites of retinal injury (Rollins, 1997; Lu et al., 1998; Deshmane et al., 2009). Deletion of CCL2 disturbs the migration of MMM and dendritic cells, which in turn results in an inefficient disposal of cellular debris and an intensified inflammatory response. Several groups have examined the retina of aged mice lacking *Ccl2* or its receptor (CC chemokine receptor type 2). While some reported that these mice exhibit signs of retinal and RPE degeneration (Ambati et al., 2003; Chen et al., 2011), others observed only increased subretinal MMM cells but no retinal degeneration in the knockout animals (Luhmann et al., 2009, 2013).

The identification of risk alleles for age-related macular degeneration in the complement system highlights the importance of normal complement activity for maintenance of the outer retina (Fritsche et al., 2013). One of the most potent alleles is complement factor H, which acts to regulate complement activity (Shaw et al., 2012). Decay accelerating factor (DAF) also plays a central role in regulating activity of the classical, alternative and lectin complement pathways (Medof et al., 1984; Sun et al., 1999). DAF regulates the complement cascade on the cell surface through interactions with C4b in the classical and lectin complement pathways, and with C3b in the alternative complement pathway (Medof et al., 1984). In addition, DAF dissociates C3 convertase molecules into constituent subunits to protect self-cells from complement-mediated injury (Ito et al., 1989). In the classic and lectin pathways, DAF cleaves C3 convertase by disassociating C2a from C4b. In the alternative pathway, DAF deactivates C3 convertase in the following steps. The proteolytic component of the C3 convertase (C3bBb), Bb, is first removed, after which C3b is split to C3f and then to iC3b, which is further cleaved to C3c and C3dg, and finally to C3d. In addition, the association of DAF with C4b or C3b inhibits their ability to convert factor C2 or B to active C2a or Bb, respectively, thus restricting the generation of C4b2a or C3bBb, and thus formation of the membrane attack complex (MAC). DAF also inhibits the formation of the highly proinflammatory anaphylatoxins C3a and C5a. Therefore, the absence of DAF is anticipated to result in increased complement activation, increased MAC formation, and consequent membrane disruption. In the present study, we examined the outer retina in single and double mutants for *Ccl2* (Lu et al., 1998) and/or *Daf1* (Lin et al., 2001, 2002). We report that single mutants develop a mild degenerative phenotype, based on multiple measures of outer retinal function and structure. In comparison, our data document that mice lacking both *Ccl2* and *Daf1* develop a much more severe phenotype, indicating a destructive synergism between these gene deletion models. In addition, $Ccl2^{-/-}/Daf1^{-/-}$ mice have increased endoplasmic reticulum (ER) stress compared to C57BL/6J mice.

2. Materials and methods

2.1. Animals

All animal procedures were approved by the Institutional Animal Care and Use Committee of Cleveland Clinic and were conducted in accordance with the ARVO Statement for the Use of Animals in Ophthalmic and Vision Research. *Ccl2*$^{-/-}$ (JAX #004434) mice and C57BL/6J (JAX #000664) mice were purchased from the Jackson Laboratory (Bar Harbor, Maine). *Daf1*$^{-/-}$ mice (Lin et al., 2001) were backcrossed with C57BL/6J mice for more than 12 generations. *Ccl2*$^{-/-}$/*Daf1*$^{-/-}$ mice were generated by crossbreeding *Ccl2*$^{-/-}$ mice and *Daf1*$^{-/-}$ mice. In view of the recent report that the *Crb1*^{rd8} allele is present in many mouse strains (Mehalow et al., 2003), we verified that this allele was not present in the mice studied here. This analysis and genotyping for the *Ccl2* and *Daf1* knockout alleles were accomplished by PCR, using published protocols (Rovin et al., 1999; Lin et al., 2001; Mehalow et al., 2003).

2.2. Fundus imaging

Ocular imaging was performed in anesthetized mice using a scanning laser ophthalmoscope (Model HRA2, Heidelberg Engineering, Carlsbad, CA). A manual z-axis focus adjustment permitted collection of retinal images from the RPE-photoreceptor interface using infrared-darkfield (SLO-IRDF) and autofluorescence (SLO-AF) imaging modes which employ illumination/excitation wavelengths of 820 and 488 nm, respectively. Online algorithms within the HRA2 system software enabled automatic real-time tracking (ART) and mean averaging of sequentially collected images to further enhance signal-to-noise ratio (SNR), especially when using AF-SLO mode. A sequence of 25 individual image frames was averaged using the HRA2 ART feature to improve SNR of the AF-SLO images. Image J was used to manually count the total number of autofluorescent foci (AFF) observed in each SLO-AF image to obtain a mean number for each eye.

2.3. Electroretinography

After overnight dark adaptation, mice were anesthetized with a mixture of ketamine (80 mg/kg) and xylazine (16 mg/kg) diluted in saline. The pupils were dilated with eye drops (1% mydriacyl, 1% cyclopentolate HCl, 2.5% phenylephrine HCl) and the corneal surface was anesthetized with 0.5% proparacaine HCl eye drops. Mice were placed on a temperature-regulated heating pad during the ERG recording session. ERGs were recorded from the corneal surface with a series of stimulus intensities. ERGs were recorded using a stainless steel electrode that made contact with the center of corneal surface through a thin layer of 0.7% methylcellulose. Needle electrodes were subcutaneously inserted into the cheek and the tail as reference and ground leads, respectively. Stimuli ranged from −3.6 to 2.1 log cd s/m^2 and were presented in increasing order. The ERG responses were digitized at 2000 Hz, differentially amplified (0.3–1500 Hz), averaged and stored using a UTAS-E3000 Electrophysiology System (LKC Technologies, Gaithersburg, MD, USA). A notch filter at 60 Hz was used during dark-adapted ERG recordings. The amplitude of the a-wave was measured at 8 ms after flash stimulation from the pre-stimulus baseline; the b-wave amplitude was measured from baseline or from the a-wave trough.

2.4. Histological analysis

After sacrifice, eyes were enucleated and immediately fixed with 4% paraformaldehyde in phosphate buffered saline (PBS) for 30 min. The cornea and lens were then dissected and the eyes were fixed for an additional 4 h in 4% paraformaldehyde in PBS, and then processed through a graded series of sucrose in PBS solutions: 10% for 1 h, 20% for 1 h, and 30% overnight. The eyes were embedded in Optimal Cutting Temperature (OCT) compound (Sukura Finetek, Torrance, CA), frozen on dry ice, and stored at −80 °C. Frozen sections (5 μm) were cut sagittally, passing through the optic nerve head, and stained with hematoxylin and eosin. Photographs were taken on either side of the optic nerve head using an Olympus BX 60 microscope (20x), and the thicknesses of the outer nuclear layer (ONL) and inner nuclear layer (INL) were measured at 200 μm from the edge of the optic disc using ImageJ 1.48v software (National Institutes of Health, MD) by an examiner who was blinded to genotype. For each mouse, values indicate the average of three consecutive sections.

2.5. Detection of apoptotic cells by terminal deoxynucleotidyl transferase dUTP nick end labeling (TUNEL)

Apoptosis was examined using the *In Situ* Cell Death Detection Kit, TMR red (Roche Applied Science, Indianapolis, IN). 10 μm retinal sections were prepared as described above in Section 2.4, and were then incubated with freshly prepared 0.1% Triton X-100/ 0.1% sodium citrate permeabilization solution for 2 min on ice. After rinsing with PBS 3 times, the sections were incubated with the TUNEL reaction mixture for 60 min at 37 °C in the dark and then rinsed with PBS 3 times. Sections were mounted with VECTA-SHIELD Mounting Medium with DAPI (Burlingame, CA), sealed with HistoSeal Laboratory Sealant (BioWorld, Dublin, OH) and visualized with the fluorescence microscope. For each section, the number of TUNEL-positive cells within the INL and the ONL was counted within a 20x field (426 μm in length) located on either side of the optic nerve. The values from separate sections obtained within a given eye were averaged to derive a single value for that eye.

2.6. Immunohistochemistry

Immunofluorescence staining was used to examine expression of the following proteins: glucose-regulated protein 78 (GRP78), activating transcription factor 4 (ATF4), mitogen-activated protein kinase (MAPK) p-p38, p-ERK, p-JNK, p–NF–κB p65 and SIRT1. The retina sections were prepared by the same procedure mentioned in 2.4. Sections were cut with thickness of 10 μm on a cryostat and incubated in PBS containing 5% normal goat serum, 1% BSA and 0.5% Triton X-100 for 1 h to block non-specific binding, followed by incubation with primary antibodies (anti-GRP78 BiP antibody, 1:400, ab21685 Abcam, Cambridge, MA; anti-ATF4, 1:120, SC-200 Santa Cruz Biotechnology, Dallas, TX; anti-phospho-ERK, ab76165, anti-phospho-JNK, ab124956, anti-phospho-p38 MAPK, 1:500, ab4822 Abcam, Cambridge, MA; anti-phospho-p65 NF-κB, 1:150, ab86299, Abcam, Cambridge, MA; anti-SIRT1, 1:50 ab12193, Abcam, Cambridge, MA) overnight at 4 °C. After three washes with PBS, the sections were incubated with goat anti-rabbit IgG H&L Alexa Fluo® 555 (1:600, ab150086, Abcam, Cambridge, MA) 2 h at room temperature. After washing with PBS, sections were mounted with VECTASHIELD mounting medium with DAPI and examined under a fluorescent microscope Olympus BX53.

2.7. Statistical analysis

For the analysis of ERG data, repeated measures ANOVA was used. The power analysis was conducted by the F-test of one-way ANOVA, where we considered numbers as outcome and groups as the factor. For the analysis of SLO images, one-way ANOVA with Tukey's multiple comparisons test. All other comparisons between C57BL/6J and mutant data were made using two-tailed, unpaired Student's t-tests. For all statistical comparisons, $p < 0.05$ was considered significant.

For the analysis of histological data, TUNEL data and SLO data, one-way ANOVA was used to compare the difference between the four groups.

3. Results

3.1. SLO fundus image

SLO-IRDF imaging at 820 nm of the retinas showed no appreciable morphologic differences among C57BL/6J, *Ccl2*$^{-/-}$/*Daf1*$^{-/-}$, *Ccl2*$^{-/-}$, and *Daf1*$^{-/-}$ mice (Fig. 1A top panels). SLO-AF imaging at 488 nm, however, revealed an increased number of AFF in all three mutant strains compared to C57BL/6J (Fig. 1A, bottom panels). The SLO-AF AFF count was significantly higher in *Ccl2*$^{-/-}$/*Daf1*$^{-/-}$ (Fig. 1B, all $p < 0.05$).

3.2. Electroretinography

We used dark-adapted ERGs to compare outer retinal function of C57BL/6J and mutant mice at 12 months of age. Fig. 2A presents representative responses obtained from each genotype. In each mutant strain, the ERGs had a normal waveform but were of reduced amplitude. Fig. 2B presents luminance-response functions for the major ERG components. In comparison to C57BL/6J mice, ERGs were smaller in mutant mice. The reduction of the ERG a-wave amplitude was significant in *Ccl2*$^{-/-}$ ($p = 0.041$) and *Ccl2*$^{-/-}$/*Daf1*$^{-/-}$ mice ($p = 0.004$), but not in *Daf1*$^{-/-}$ mice ($p = 0.058$). While the a-wave reduction was more pronounced in *Ccl2*$^{-/-}$/*Daf1*$^{-/-}$ than in the single mutants, this difference was not significant ($p = 0.305$ for *Ccl2*$^{-/-}$/*Daf1*$^{-/-}$ vs. *Ccl2*$^{-/-}$; $p = 0.129$ for *Ccl2*$^{-/-}$/*Daf1*$^{-/-}$ vs. *Daf1*$^{-/-}$). The amplitude reduction of the b-wave was significant in *Ccl2*$^{-/-}$ ($p = 0.025$) and *Ccl2*$^{-/-}$/*Daf1*$^{-/-}$ ($p = 0.001$) mice, but not in *Daf1*$^{-/-}$ mice ($p = 0.067$). Comparisons between the mutant strains were not significant (all $p > 0.05$). These results indicate that outer retinal function is reduced in mice lacking CCL2 and that the magnitude of this reduction is enhanced when mice also lack DAF, while the absence of DAF alone has less of an impact.

3.3. Histological analysis

Fig. 3A presents representative sections of C57BL/6J, *Ccl2*$^{-/-}$/*Daf1*$^{-/-}$, *Ccl2*$^{-/-}$, and *Daf1*$^{-/-}$ mice. The thickness of the ONL and INL were significantly reduced in *Ccl2*$^{-/-}$/*Daf1*$^{-/-}$ mice as compared to C57BL/6J or the single mutants. In comparison, the retinas of *Ccl2*$^{-/-}$ and *Daf1*$^{-/-}$ mice had more modest changes. Fig. 3B summarizes measures of ONL and INL thickness. The ONL and INL were significantly thinner in the retina of *Ccl2*$^{-/-}$/*Daf1*$^{-/-}$ mice as compared to the other three genotypes (all $p < 0.01$). None of the other comparisons of ONL or INL thickness were significantly different between C57BL/6J and single mutant animals (all $p > 0.05$).

3.4. Detection ofapoptotic cells by TUNEL

Cellular apoptosis was tested by TUNEL analysis. Fig. 4A shows representative images of TUNEL staining in C57BL/6J, *Ccl2*$^{-/-}$/*Daf1*$^{-/-}$, *Ccl2*$^{-/-}$ and *Daf1*$^{-/-}$ retinas. In comparison to C57BL/6J, the number of TUNEL positive cells was increased in *Ccl2*$^{-/-}$ and *Daf1*$^{-/-}$ retinas, in both the ONL and INL. The greatest numbers of TUNEL-positive cells were seen, however, in *Ccl2*$^{-/-}$/*Daf1*$^{-/-}$ retinas, with a similar distribution between the ONL and INL. Fig. 4B summarizes the TUNEL results. The number of TUNEL-positive cells was significantly higher in both the ONL and the INL of *Ccl2*$^{-/-}$/*Daf1*$^{-/-}$ retinas as compared to the other three groups (all $p < 0.01$). The pairwise comparisons between the other groups were not significant (all $p > 0.05$). The magnitude of the increase of TUNEL positive cells corresponds to the extent to which the thickness of the ONL and INL were decreased (Fig. 4B), indicating that the absence of CCL2 and/or DAF leads to cell death through an apoptotic pathway.

3.5. Increased expression of GRP78 and ATF4 in the retinas of Ccl2$^{-/-}$/Daf1$^{-/-}$ mice

In view of recent evidence that increased ER stress results in apoptosis contributing to photoreceptor degeneration in other mouse models (Zhang et al., 2014), we examined the levels of the ER stress markers GRP78 and ATF4 using immunostaining. For these studies, we focused on the *Ccl2*$^{-/-}$/*Daf1*$^{-/-}$ retina which shows a more severe phenotype of retinal degeneration than the single knockouts (Figs. 1–4). Our results show that the expression of GRP78, a major ERchaperone that facilitates protein folding, was increased in the INL and GCL as well as in the photoreceptor inner segment (IS) of the *Ccl2*$^{-/-}$/*Daf1*$^{-/-}$ retina, compared to the C57BL/ 6J retina. In C57BL/6J retinas, we observed weak staining for ATF4, a main transcription factor involved in the ER stress response (also known as the unfolded protein response, UPR) in the INL and GCL. In comparison, strong ATF4 immunoreactivity was observed in *Ccl2*$^{-/-}$/*Daf1*$^{-/-}$ retinas, with the strongest signals seen in the nuclei of cells in the INL and GCL (Fig. 5).

3.6. Upregulation of phosphor-ERK, phosphor-JNK, phosphor-p38 MAPK and phosphor-p65 and downregulation ofSIRT1 in the retina of Ccl2$^{-/-}$/Daf1$^{-/-}$ mice

MAPKs are a group of threonine/serine-specific protein kinases that are used widely in regulating gene expression, apoptosis and cell survival (Pearson et al., 2001). There are three well-defined subgroups of MAPKs: the extracellular signal regulated kinases (ERKs), the c-Jun N-terminal kinases (JNKs), and the p38 MAPKs. They are activated by phosphorylation events secondary to a variety of different stresses and inflammatory cytokines (Rouse et al., 1994; Zarubin and Han, 2005; Coulthard et al., 2009; Wagner and Nebreda, 2009). Sustained MAPK activation can cause excessive generation of MAPK-regulated genes, uncontrolled proliferation and cell death (Mansouri et al., 2003). We examined the distribution of phosphorylated ERK (p-ERK),JNK (p-JNK) and p38 (p-p38) in C57BL/6J and *Ccl2*$^{-/-}$/*Daf1*$^{-/-}$ retinas (Fig. 6). In comparison to C57Bl/6J, the levels of p-ERK were elevated in the IS and GCL layers (Fig. 6, upper row), of p-JNK were elevated intheOPL(Fig. 6, middle row), and of p-p38 were elevated in the INL, GCL and in the retinal pigment epithelium (Fig. 6, lower row).

NF-κB (Nuclear Factor-KappaB) is a heterodimeric protein consisted of NF-KappaB1 (p50), NF-KappaB2 (p52), and members of the Rel family of transcription factors: RelA (p65), RelB, and c-Rel (Rel) (Hayden and Ghosh, 2004). In non-stressed cells, NF-κB resides in the cytosol bound to its inhibitor (IκB), and Rel expression is low, while elevated expression of Rel/NF-κB is observed in ER stress (Hung et al., 2004) and oxidative stress (Li and Karin, 1999). Our data shows that the levels of the activated form of p65 (p-p65) were elevated in the INL and GCL of the *Ccl2*$^{-/-}$/*Daf1*$^{-/-}$ retina compared to C57BL/6J mice (Fig. 7).

SIRT1 (Sirtuin Type 1) is a member of the mammalian sirtuin family that generates enzyme activity in a NAD^+-dependent way to deacetylate histones and prolong cell survival (Rahman and Islam, 2011). Numerous protein targets can be deacetylated by SIRT1, thereby regulating multiple cellular pathways related to stress responses, apoptosis, inflammation and metabolism (Ozawa et al., 2010). For example, SIRT1 can downregulate the gene expression of NF-κB and the cellular apoptosis gene Bax (Zheng et al., 2012) respectively. SIRT1 also deacetylates the DNA repair factor Ku70, which acts to separate the proapoptotic factor Bax from mitochondria, thereby protecting the cell from apoptosis (Cohen et al., 2004). Our data shows that SIRT1 is localized to the IS of the C57BL/6J retina and that SIRT1 levels are reduced in *Ccl2*$^{-/-}$/*Daf1*$^{-/-}$ mice (Fig. 7). Determining how this reduction in SIRT1 contributes to the retinal degenerative process will require further study, but may relate to its role in inhibition of ER stress (Ghosh et al., 2011; Lee et al., 2014; Melhem et al., 2015) and its demonstrated protective role when upregulated on retinal neurons (Mimura et al., 2013).

4. Discussion

In the present study, we examined the outer retina of mice lacking the complement regulator DAF and/or the chemokine ligand CCL2. We focused on 1 year old mice, to allow even slow age-related changes to become apparent. We report that mice lacking only CCL2 or DAF have a modest phenotype, comprised of elevated autofluorescence and reduced ERG amplitude. While the phenotype is mild, these results support a role for CCL2 and DAF in maintenance of the outer retina. A more striking phenotype was observed in mice lacking both CCL2 and DAF. All of the abnormalities observed in single mutants were accentuated in the double mutant retina, indicating that the defects associated with CCL2 or DAF synergize when both are absent.

Mice lacking only CCL2 had modest retinal changes. We did not see a significant reduction in the thickness of the ONL or INL nor an increase in the total number of apoptotic cells. Overall, our data is consistent with the results of Luhmann et al. (2009) who observed that the *Ccl2*$^{-/-}$ retina remained generally normal up to 25 months of age, with the exception of an increased accumulation of macrophages in the subretinal space that were apparent as AFFs. As suggested in that study (Luhmann et al., 2009), the mild retinal phenotype of *Ccl2*$^{-/-}$ mice may reflect the ability of another che-moattractant, such as chemokine (C-X-C motif) ligand 2 (CXCL2) (Raoul et al., 2010), to replace some of the normal functions of CCL2. There are several possible explanations for the different reports regarding the impact of *Ccl2* deletion on the mouse retina (Ambati et al., 2003; Luhmann et al., 2009, 2013; Chen

et al., 2011). It is important to bear in mind that most of the studies, including the present one, report that the *Ccl2*$^{-/-}$ retinal phenotype is relatively mild. Perhaps the simplest explanation, therefore, is that the experimental techniques used by these different laboratories may have different sensitivity to detect an abnormal phenotype. Alternatively, it is possible that the phenotype is influenced by the background strain against which the mutant allele was expressed.

Mice only lacking DAF also had a limited retinal phenotype. Although *Daf1*$^{-/-}$ mice have marked changes in multiple systems following challenge with various factors (Fang et al., 2007; Toomey et al., 2010), when we examined 1-year old *Daf1*$^{-/-}$ retinas, we did not see significant changes in the retinas of *Daf1*$^{-/-}$ mice. These results indicate that the role of DAF in regulating MAC activity may be partially achieved by another complement regulator, such as membrane cofactor protein (CD46) (Davies et al., 1994; Ebrahimi et al., 2014) or MAC-inhibitory protein (CD59), or may not be critical when mice are reared in an environment where everything they consume and contact has been sterilized. In future studies, it would be interesting to see if the *Daf1*$^{-/-}$ retina has an abnormal response to an extrinsic or intrinsic challenge.

Of all the mouse stains examined here, *Ccl2*$^{-/-}$/*Daf1*$^{-/-}$ mice displayed the greatest retinal changes. These include significant reductions in ERG amplitude reflecting loss of cells in the ONL due to increased rates of apoptosis. Apoptosis was not limited to the ONL, as a high level of TUNEL positive cells was also seen in the INL of *Ccl2*$^{-/-}$/*Daf1*$^{-/-}$ mice. *Ccl2*$^{-/-}$/*Daf1*$^{-/-}$ mice also displayed higher numbers of AFFs in the subretinal space, significant upregulation of phosphorylation of p38, ERK, JNK and p65, significant increase of the expression of GRP78 and ATF4 with more intensive staining in the INL and GCL, suggesting an elevated ER stress in the mutant retina. These changes are consistent with the wide distribution of DAF in the retina, from the OPL to the GCL (Williams et al., 2013), and suggests that the phenotype associated with DAF deficiency is exacerbated when combined with CCL2 deficiency, which may increase the activity of complement pathways, and, in turn, elevate ER stress (Kunchithapautham et al., 2014; Cybulsky et al., 2002). In support of this scenario, other laboratories have shown that ER stress contributes to RPE and retinal cell degeneration in animal models of age-related macular degeneration (Libby and Gould, 2010; Salminen et al., 2010; Zhang et al., 2014) or photoreceptor degeneration caused by genetic (i.e., rhodopsin mutations including S334ter, RCS, P23H-3, and hT17M) or environmental (i.e., intensive light exposure) factors (Lin et al., 2007; Gorbatyuk and Gorbatyuk, 2013; Kroeger et al., 2012; Kunte et al., 2012; Shinde et al., 2012). As reviewed previously, ER stress activates signaling pathways of the UPR to regulate cellular activity and cell fate in stress conditions (Jing et al., 2012; Zhang et al., 2014, 2015). While physiological or mild ER stress can be overcome by the UPR, an adaptive mechanism to reduce ER stress, pathological (persistent and intensive) ER stress will activate the apoptotic process leading to cell death and degeneration. In addition, chronic ER stress has been shown to promote inflammatory response, at least in part, through activation of JNK and NF-κB (Zheng et al., 2012). Indeed, we observed that increased apoptosis was accompanied byJNK and NF-κB activation in the INLand ONLof *Ccl2*$^{-/-}$/*Daf1*$^{-/-}$ retinas. Taken together, these results suggest an important role of ER stress in the ONL and INL apoptosis noted in *Ccl2*$^{-/-}$/*Daf1*$^{-/-}$ mice.

The upregulation of p-p38, p-ERK, p-JNK in *Ccl2*$^{-/-}$/*Daf1*$^{-/-}$ mice also indicates a widespread activation of cell defense pathways (Zarubin and Han, 2005), related to oxidative stress (Gaitanaki et al., 2003) or inflammation (Kaminska, 2005). ER stress and oxidative stress can interact with each other (Malhotra and Kaufman, 2007). In addition, ER stress can also activate MAPK pathways, in which MAPKs mediate the cytotoxicity induced by the ER stress (Darling and Cook, 2014). MAPK activation is required to induce autophagy after ER stress (Kim et al., 2010), and MAPKs interact with SIRT1 in response to cellular stress (Zhao et al., 2012; Becatti et al., 2014). Low levels of SIRT1 can increase the activity of NF-κB pathway (Salminen et al., 2013). Moreover, SIRT1 plays an antioxidant role through the FOXO family, by increasing the ability of FOXO3 to induce cell cycle arrest and increasing resistance to oxidative stress while inhibiting the ability of FOXO3 acetylation or phosphorylation to induce cell death (Brunet et al., 2004). Furthermore, SIRT1 regulates DNA stability and promotes cell survival through Ku70, a nonhomologous end-joining DNA repair protein and p53-dependent apoptosis (Cheng et al., 2003). SIRT1 also inhibits apoptosis by deacetylating Ku70 and reducing the disruption of Ku70-Bax interaction, allowing Bax to move away from mitochondria (Cohen et al., 2004). It will be important to determine which of these roles might connect the decreased levels of SIRT1 with the increased apoptosis noted in *Ccl2*$^{-/-}$/*Daf1*$^{-/-}$ retinas.

In summary, CCL2 or DAF1 single deletion does not cause marked retinal degeneration, due perhaps to compensation by other protective mechanisms. However, loss of CCL2 and DAF1 results in a significant phenotype with increased ER stress and oxidative stress, activation of apoptosis signaling pathways (Tabas and Ron, 2011; Szegezdi et al., 2006; Kannan and Jain, 2000) and cell death. This model may be useful for the evaluation of treatments designed to slow retinal cell death by reduction of cellular stress.

Acknowledgments

This work was supported by the BrightFocus Foundation, the National Eye Institute (EY019949, EY025061), the Foundation Fighting Blindness, VA Medical Research Service, and by unrestricted grants from Research to Prevent Blindness to the Departments of Ophthalmology of the Cleveland Clinic Lerner College of Medicine of Case Western Reserve University and SUNY-Buffalo.

The authors thank Prof. Feng Lin, Department of Immunology, Lerner Research Institute, Cleveland Clinic for providing Daf1 mutant mice.

References

Ambati J, Anand A, Fernandez S, Sakurai E, Lynn BC, Kuziel WA, Rollins BJ, Ambati BK. An animal model of age-related macular degeneration in senescent Ccl-2- or Ccr-2-deficient mice. Nat. Med. 2003; 9:1390–1397. [PubMed: 14566334]

Becatti M, Fiorillo C, Barygina V, Cecchi C, Lotti T, Prignano F, Silvestro A, Nassi P, Taddei N. SIRT1 regulates MAPK pathways in vitiligo skin: insight into the molecular pathways of cell survival. J. Cell. Mol. Med. 2014; 18:514–529. [PubMed: 24410795]

Brunet A, Sweeney LB, Sturgill JF, Chua KF, Greer PL, Lin Y, Tran H, Ross SE, Mostoslavsky R, Cohen HY, Hu LS, Cheng HL, Jedrychowski MP, Gygi SP, Sinclair DA, Alt FW, Greenberg ME. Stress-dependent regulation of FOXO transcription factors by the SIRT1 deacetylase. Science. 2004; 303:2011–2015. [PubMed: 14976264]

Chen M, Forrester JV, Xu H. Dysregulation in retinal para-inflammation and age-related retinal degeneration in CCL2 or CCR2 deficient mice. PLoS One. 2011; 6:e22818. [PubMed: 21850237]

Cheng HL, Mostoslavsky R, Saito S, Manis JP, Gu Y, Patel P, Bronson R, Appella E, Alt FW, Chua KF. Developmental defects and p53 hyper-acetylation in Sir2 homolog (SIRT1)-deficient mice. Proc. Natl. Acad. Sci. USA. 2003; 100:10794–10799. [PubMed: 12960381]

Cohen HY, Miller C, Bitterman KJ, Wall NR, Hekking B, Kessler B, Howitz KT, Gorospe M, de Cabo R, Sinclair DA. Calorie restriction promotes mammalian cell survival by inducing the SIRT1 deacetylase. Science. 2004; 305:390–392. [PubMed: 15205477]

Coulthard LR, White DE, Jones DL, McDermott MF, Burchill SA. p38(MAPK): stress responses from molecular mechanisms to therapeutics. Trends Mol. Med. 2009; 15:369–379. [PubMed: 19665431]

Cybulsky AV, Takano T, Papillon J, Khadir A, Liu J, Peng H. Complement C5b-9 membrane attack complex increases expression of endoplasmic reticu-lum stress proteins in glomerular epithelial cells. J. Biol. Chem. 2002; 277:41342–41351. [PubMed: 12191998]

Darling NJ, Cook SJ. The role of MAPK signalling pathways in the response to endoplasmic reticulum stress. Biochim. Biophys. Acta. 2014; 1843:2150–2163. [PubMed: 24440275]

Davies ME, Horner A, Loveland BE, McKenzie IF. Upregulation of complement regulators MCP (CD46), DAF (CD55) and protectin (CD59) in arthritic joint disease. Scand. J. Rheumatol. 1994; 23:316–321.

Deshmane SL, Kremlev S, Amini S, Sawaya BE. Monocyte chemo-attractant protein-1 (MCP-1): an overview. J. Interferon Cytokine Res. 2009; 29:313–326. [PubMed: 19441883]

Ebrahimi KB, Fijalkowski N, Cano M, Handa JT. Oxidized low-density-lipoprotein-induced injury in retinal pigment epithelium alters expression of the membrane complement regulatory ractors CD46 and CD59 through exo-somal and apoptotic bleb release. Adv. Exp. Med. Biol. 2014; 801:259–265. [PubMed: 24664706]

Fang C, Miwa T, Shen H, Song WC. Complement-dependent enhancement of CD8+ T cell immunity to lymphocytic choriomeningitis virus infection in decay-accelerating factor-deficient mice. J. Immunol. 2007; 179:3178–3186. [PubMed: 17709533]

Fritsche LG, Chen W, Schu M, Yaspan BL, Yu Y, Thorleifsson G, et al. Seven new loci associated with age-related macular degeneration. Nat. Genet. 2013; 45:433–439. [PubMed: 23455636]

Gaitanaki C, Konstantina S, Chrysa S, Beis I. Oxidative stress stimulates multiple MAPK signalling pathways and phosphorylation of the small HSP27 in the perfused amphibian heart. J. Exp. Biol. 2003; 206:2759–2769. [PubMed: 12847121]

Ghosh HS, Reizis B, Robbins PD. SIRT1 associates with eIF2-alpha and regulates the cellular stress response. Sci. Rep. 2011; 1:150–159. [PubMed: 22355666]

Gorbatyuk M, Gorbatyuk O. Review: retinal degeneration: focus on the unfolded protein response. Mol. Vis. 2013; 19:1985–1998. [PubMed: 24068865]

Hayden MS, Ghosh S. Signaling to NF-kappaB. Genes. Dev. 2004; 18:2195–2224. [PubMed: 15371334]

Hung JH, Su IJ, Lei HY, Wang HC, Lin WC, Chang WT, Huang W, Chang WC, Chang YS, Chen CC, Lai MD. Endoplasmic reticulum stress stimulates the expression of cyclooxygenase-2 through activation of NF-kappaB and pp38 mitogen-activated protein kinase. J. Biol. Chem. 2004; 279:46384–46392. [PubMed: 15319438]

Ito S, Tamura N, Fujita T. Effect of decay-accelerating factor on the assembly of the classical and alternative pathway C3 convertases in the presence of C4 or C3 nephritic factor. Immunology. 1989; 68:449–452. [PubMed: 2481642]

Jing G, Wang JJ, Zhang SX. ER stress and apoptosis: a new mechanism for retinal cell death. Exp. Diabetes Res. 2012; 2012:589589. http://dx.doi.org/10.1155/2012/589589. [PubMed: 22216020]

Kaminska B. MAPK signalling pathways as molecular targets for anti-inflammatory therapy-from molecular mechanisms to therapeutic benefits. Biochim. Biophys. Acta. 2005; 1754:253–262. [PubMed: 16198162]

Kannan K, Jain SK. Oxidative stress and apoptosis. Pathophysiology. 2000; 7:153–163. [PubMed: 10996508]

Kim DS, Kim JH, Lee GH, Kim HT, Lim JM, Chae SW, Chae HJ, Kim HR. p38 Mitogen-activated protein kinase is involved in endoplasmic retic-ulum stress-induced cell death and autophagy in human gingival fibroblasts. Biol. Pharm. Bull. 2010; 33:545–549. [PubMed: 20410583]

Kroeger H, Messah C, Ahern K, Gee J, Joseph V, Matthes MT, Yasumura D, Gorbatyuk MS, Chiang WC, LaVail MM, Lin JH. Induction of endo-plasmic reticulum stress genes, BiP and chop, in genetic and environmental models of retinal degeneration. Invest. Ophthalmol. Vis. Sci. 2012; 53:7590–7599. [PubMed: 23074209]

Kunchithapautham K, Atkinson C, Rohrer B. Smoke exposure causes endoplasmic reticulum stress and lipid accumulation in retinal pigment epithelium through oxidative stress and complement activation. J. Biol. Chem. 2014; 289:14534–14546. [PubMed: 24711457]

Kunte MM, Choudhury S, Manheim JF, Shinde VM, Miura M, Chiodo VA, Hauswirth WW, Gorbatyuk OS, Gorbatyuk MS. ER stress is involved in T17M rhodopsin-induced retinal degeneration. Invest. Ophthalmol. Vis. Sci. 2012; 53:3792–3800. [PubMed: 22589437]

Lee J, Hong SW, Park SE, Rhee EJ, Park CY, Oh KW, Park SW, Lee WY. Exendin-4 attenuates endoplasmic reticulum stress through a SIRT1-dependent mechanism. Cell. Stress Chaperones. 2014; 19:649–656. [PubMed: 24446069]

Libby RT, Gould DB. Endoplasmic reticulum stress as a primary pathogenic mechanism leading to age-related macular degeneration. Adv. Exp. Med. Biol. 2010; 664:403–409. [PubMed: 20238041]

Lin F, Emancipator SN, Salant DJ, Medof ME. Decay-accelerating factor confers protection against complement-mediated podocyte injury in acute nephrotoxic nephritis. Lab. Invest. 2002; 82:563–829. [PubMed: 12003997]

Lin F, Fukuoka Y, Spicer A, Ohta R, Okada N, Harris CL, Emancipator SN, Medof ME. Tissue distribution of products of the mouse decay-accelerating factor (DAF) genes. Exploitation of a Daf1 knock-out mouse and site-specific monoclonal antibodies. Immunology. 2001; 104:215–225. [PubMed: 11683962]

Lin JH, Li H, Yasumura D, Cohen HR, Zhang C, Panning B, Shokat KM, Lavail MM, Walter P. IRE1 signaling affects cell fate during the unfolded protein response. Science. 2007; 318:944–949. [PubMed: 17991856]

Li N, Karin M. Is NF-kappaB the sensor of oxidative stress? FASEB J. 1999; 13:1137–1143. [PubMed: 10385605]

Lu B, Rutledge BJ, Gu L, Fiorillo J, Lukacs NW, Kunkel SL, North R, Gerard C, Rollins BJ. Abnormalities in monocyte recruitment and cytokine expression in monocyte chemoattractant protein 1-deficient mice. J. Exp. Med. 1998; 187:601–608. [PubMed: 9463410]

Luhmann UF, Carvalho LS, Robbie SJ, Cowing JA, Duran Y, Munro PM, Bainbridge JW, Ali RR. Ccl2, Cx3cr1 and Ccl2/Cx3cr1 chemokine deficiencies are not sufficient to cause age-related retinal degeneration. Exp. Eye Res. 2013; 107:80–87. [PubMed: 23232206]

Luhmann UF, Robbie S, Munro PM, Barker SE, Duran Y, Luong V, Fitzke FW, Bainbridge JW, Ali RR, MacLaren RE. The drusenlike phenotype in aging Ccl2-knockout mice is caused by an accelerated accumulation of swollen autofluorescent subretinal macrophages. Invest. Ophthalmol. Vis. Sci. 2009; 50:5934–5943. [PubMed: 19578022]

Malhotra JD, Kaufman RJ. Endoplasmic reticulum stress and oxidative stress: a vicious cycle or a double-edged sword? Antioxid. Redox Signal. 2007; 9:2277–2293. [PubMed: 17979528]

Mansouri A, Ridgway LD, Korapati AL, Zhang Q, Tian L, Wang Y, Siddik ZH, Mills GB, Claret FX. Sustained activation of JNK/p38 MAPK pathways in response to cisplatin leads to Fas ligand induction and cell death in ovarian carcinoma cells. J. Biol. Chem. 2003; 278:19245–19256. [PubMed: 12637505]

Medof ME, Kinoshita T, Nussenzweig V. Inhibition of complement activation on the surface of cells after incorporation of decay-accelerating factor (DAF) into their membranes. J. Exp. Med. 1984; 160:1558–1578. [PubMed: 6238120]

Mehalow AK, Kameya S, Smith RS, Hawes NL, Denegre JM, Young JA, Bechtold L, Haider NB, Tepass U, Heckenlively JR, Chang B, Naggert JK, Nishina PM. CRB1 is essential for external limiting membrane integrity and photoreceptor morphogenesis in the mammalian retina. Hum. Mol. Genet. 2003; 12:2179–2189. [PubMed: 12915475]

Melhem, H., Hansmannel, F., Bressenot, A., Battaglia-Hsu, SF., Billioud, V., Alberto, JM., Gueant, JL., Peyrin-Biroulet, L. Methyl-deficient diet promotes colitis and SIRT1-mediated endoplasmic reticulum stress. Gut. 2015. http://dx.doi.org/10.1136/gutjnl-2014-307030. Jan 20. pii: gutjnl-2014–307030, [Epub ahead of print]

Mimura T, Kaji Y, Noma H, Funatsu H, Okamoto S. The role of SIRT1 in ocular aging. Exp. Eye. Res. 2013; 116:17–26. [PubMed: 23892278]

Ozawa Y, Kubota S, Narimatsu T, Yuki K, Koto T, Sasaki M, Tsubota K. Retinal aging and sirtuins. Ophthalmic Res. 2010; 44:199–203. [PubMed: 20829644]

Pearson G, Robinson F, Beers GT, Xu BE, Karandikar M, Berman K, Cobb MH. Mitogen-activated protein (MAP) kinase pathways: regulation and physiological functions. Endocr. Rev. 2001; 22:153–183. [PubMed: 11294822]

Rahman S, Islam R. Mammalian Sirt1: insights on its biological functions. Cell. Commun. Signal. 2011; 9:11. http://dx.doi.org/10.1186/1478-811X-9-11. [PubMed: 21549004]

Raoul W, Auvynet C, Camelo S, Guillonneau X, Feumi C, Combadière C, Sennlaub F. CCL2/CCR2 and CX3CL1/CX3CR1 chemokine axes and their possible involvement in age-related macular degeneration. J. Neuroinflammation. 2010; 7:87–93. [PubMed: 21126357]

Rollins BJ. Chemokines. Blood. 1997; 90:909–928. [PubMed: 9242519]

Rouse J, Cohen P, Trigon S, Morange M, Alonso-Llamazares A, Zamanillo D, Hunt T, Nebreda AR. A novel kinase cascade triggered by stress and heat shock that stimulates MAPKAP kinase-2 and phosphorylation of the small heat shock proteins. Cell. 1994; 78:1027–1037. [PubMed: 7923353]

Rovin BH, Lu L, Saxena R. A novel polymorphism in the MCP-1 gene regulatory region that influences MCP-1 expression. Biochem. Biophys. Res. Commun. 1999; 259:344–348. [PubMed: 10362511]

Salminen A, Kaarniranta K, Kauppinen A. Crosstalk between oxidative stress and SIRT1: impact on the aging process. Int. J. Mol. Sci. 2013; 14:3834–3859. [PubMed: 23434668]

Salminen A, Kauppinen A, Hyttinen JM, Toropainen E, Kaarniranta K. Endoplasmic reticulum stress in age-related macular degeneration: trigger for neovascularization. Mol. Med. 2010; 16:535–542. [PubMed: 20683548]

Shaw PX, Zhang L, Zhang M, Du H, Zhao L, Lee C. Complement factor H genotypes impact risk of age-related macular degeneration by interaction with oxidized phospholipids. Proc. Natl. Acad. Sci. USA. 2012; 109:13757–13762. [PubMed: 22875704]

Shinde VM, Sizova OS, Lin JH, LaVail MM, Gorbatyuk MS. ER stress in retinal degeneration in S334ter Rho rats. PLoS One. 2012; 7:e33266. [PubMed: 22432009]

Sun X, Funk CD, Deng C, Sahu A, Lambris JD, Song WC. Role of decay-accelerating factor in regulating complement activation on the erythrocyte surface as revealed by gene targeting. Proc. Natl. Acad. Sci. USA. 1999; 96:628–633. [PubMed: 9892684]

Szegezdi E, Logue SE, Gorman AM, Samali A. Mediators of endoplasmic reticulum stress-induced apoptosis. EMBO Rep. 2006; 7:880–885. [PubMed: 16953201]

Tabas I, Ron D. Integrating the mechanisms of apoptosis induced by endoplasmic reticulum stress. Nat. Cell. Biol. 2011; 13:184–190. [PubMed: 21364565]

Toomey CB, Cauvi DM, Song WC, Pollard KM. Decay-accelerating factor 1 (Daf1) deficiency exacerbates xenobiotic-induced autoimmunity. Immunology. 2010; 131:99–106. [PubMed: 20408894]

Wagner EF, Nebreda AR. Signal integration by JNK and p38 MAPK pathways in cancer development. Nat. Rev. Cancer. 2009; 9:537–549. [PubMed: 19629069]

Williams JA, Greenwood J, Moss SE. Retinal changes precede visual dysfunction in the complement factor H knockout mouse. PLoS One. 2013; 8:e68616. [PubMed: 23844226]

Zarubin T, Han J. Activation and signaling of the p38 MAP kinase pathway. Cell. Res. 2005; 15:11–18. [PubMed: 15686620]

Zhang SX, Ma JH, Bhatta M, Fliesler SJ, Wang JJ. The unfolded protein response in retinal vascular diseases: implications and therapeutic potential beyond protein folding. Prog. Retin. Eye Res. 2015; 45:111–131. [PubMed: 25529848]

Zhang SX, Sanders E, Fliesler SJ, Wang JJ. Endoplasmic reticulum stress and the unfolded protein responses in retinal degeneration. Exp. Eye Res. 2014; 125:30–40. [PubMed: 24792589]

Zhao Y, Luo P, Guo Q, Li S, Zhang L, Zhao M, Xu H, Yang Y, Poon W, Fei Z. Interactions between SIRT1 and MAPK/ERK regulate neuronal apoptosis induced by traumatic brain injury in vitro and in vivo. Exp. Neurol. 2012; 237:489–498. [PubMed: 22828134]

Zheng Z, Chen H, Li J, Li T, Zheng B, Zheng Y, Jin H, He Y, Gu Q, Xu X. Sirtuin 1-mediated cellular metabolic memory of high glucose via the LKB1/ AMPK/ROS pathway and therapeutic effects of metformin. Diabetes. 2012; 61:217–228. [PubMed: 22124463]

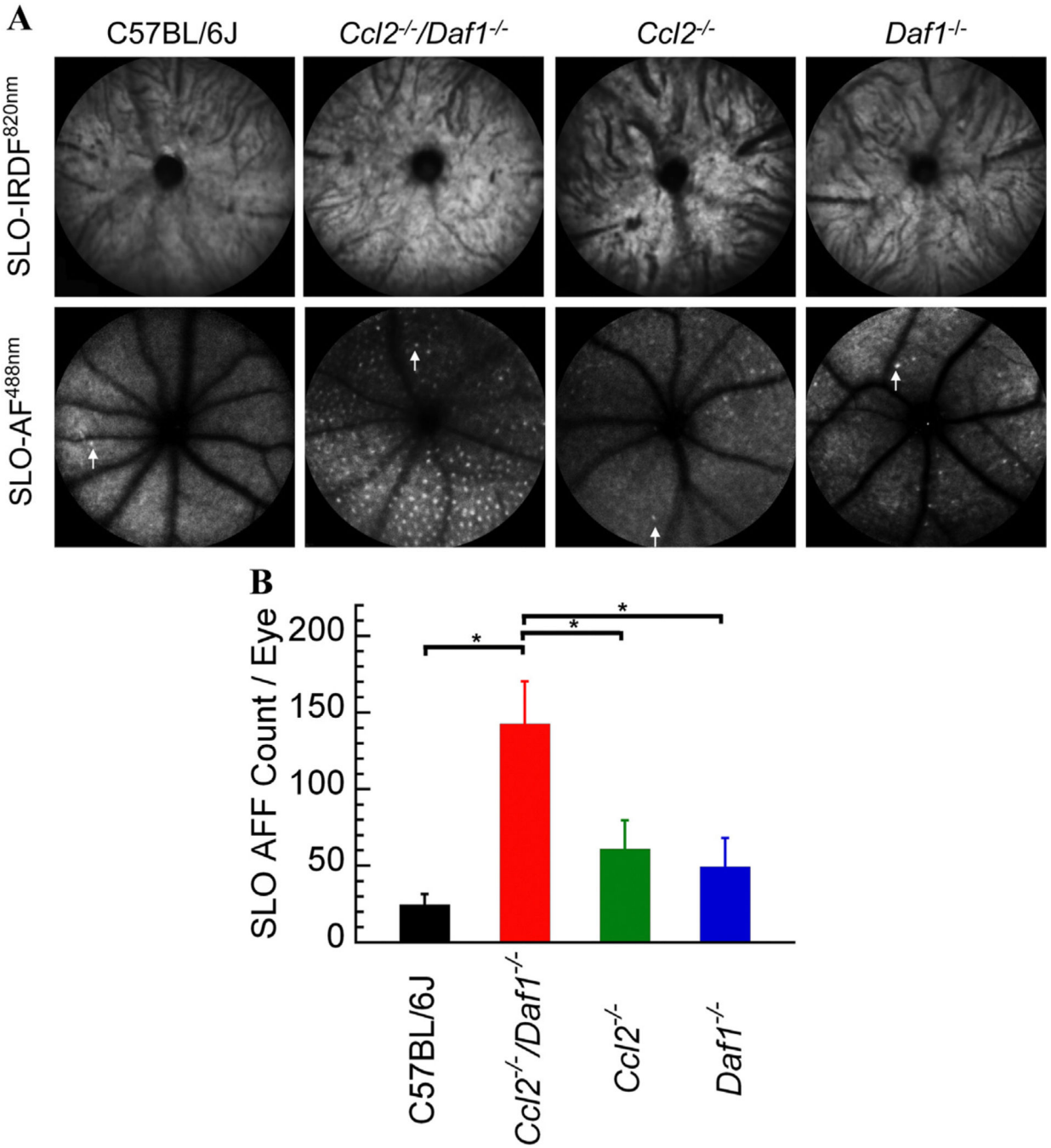

Fig. 1.

SLO imaging of mouse models studied. (**A**) Representative SLO images obtained from C57BL/6J, *Ccl2*$^{-/-}$/*Daf1*$^{-/-}$, *Ccl2*$^{-/-}$, or *Daf1*$^{-/-}$ mice. Top panels show no appreciable morphologic differences across genotypes for SLO-IRDF imaging at 820 nm. Bottom panels use SLO-AF imaging at 488 nm, which shows the (AFF) in mutant strains compared to C57BL/6J. A single AFF is indicated with an arrow in each SLO-AF488 nm image. (**B**) Numbers of SLO-AF AFF. Bars indicate the mean ± SE for 5–8 mice per genotype. The

number of SLO-AF AFF is significantly higher in $Ccl2^{-/-}/Daf1^{-/-}$ in comparison to all genotypes (all $p < 0.05$); the other comparisons are not significant.

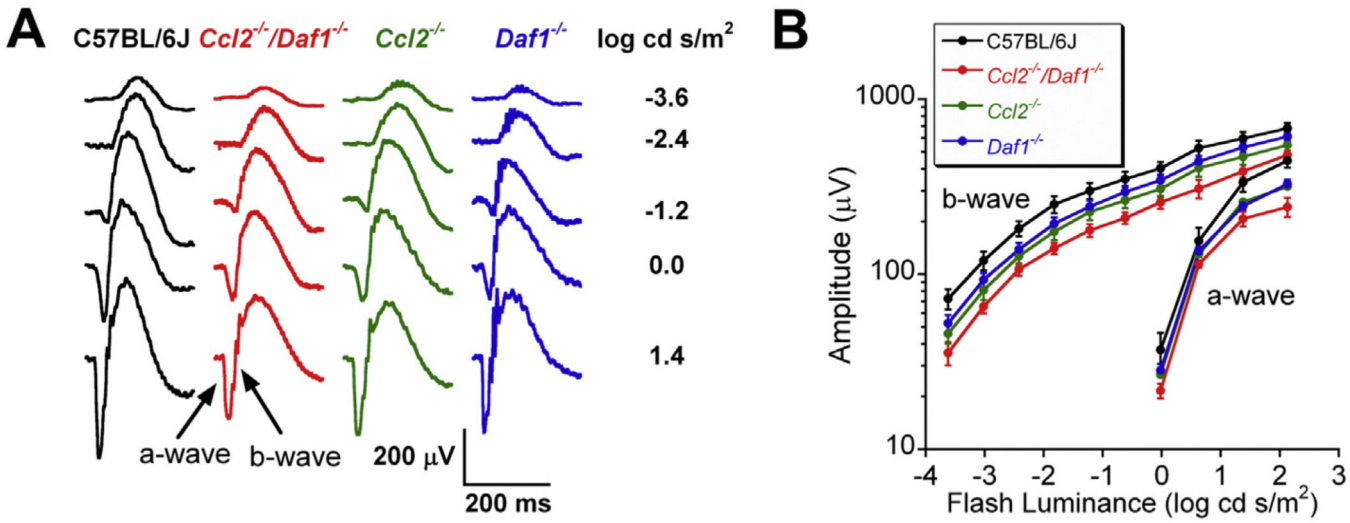

Fig. 2.

Electroretinography. (**A**) Representative waveforms obtained to strobe flash stimuli presented to the dark-adapted eyes of 12 month old mice. Stimulus strength is indicated to the right of each row of waveforms. (**B**) Luminance-response functions for a- and b-wave amplitude. Data points indicate the mean ± SE for 7–12 mice.

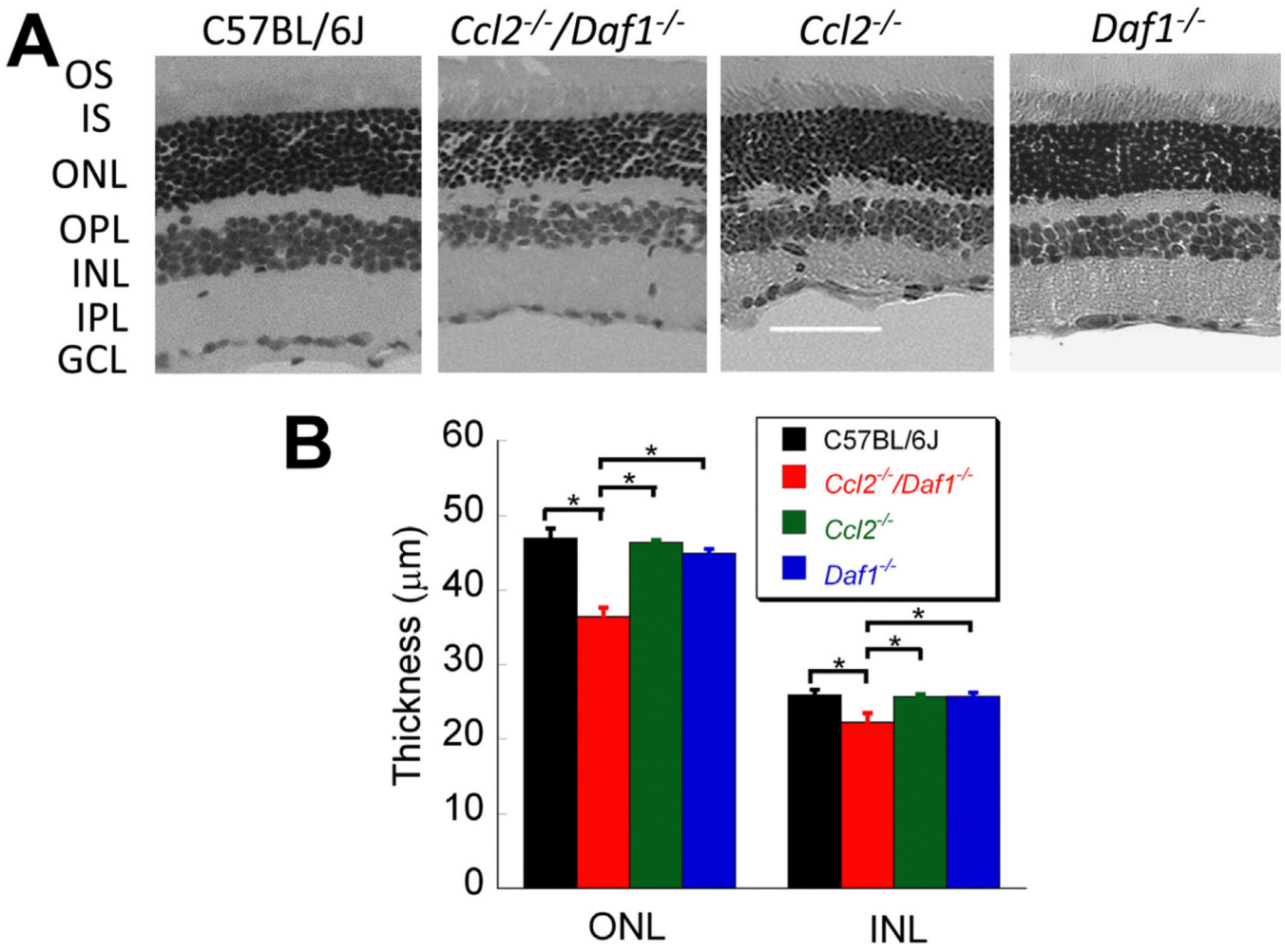

Fig. 3.

Retinal histology. (**A**) Representative hematoxylin-eosin stained images (20x) of retinal cross sections taken next to the optic nerve head. The scale bar indicates 60 μm. (**B**) Average thickness of the ONL and the INL. Bars indicate the mean ± SE for three mice per genotype. *$p < 0.01$.

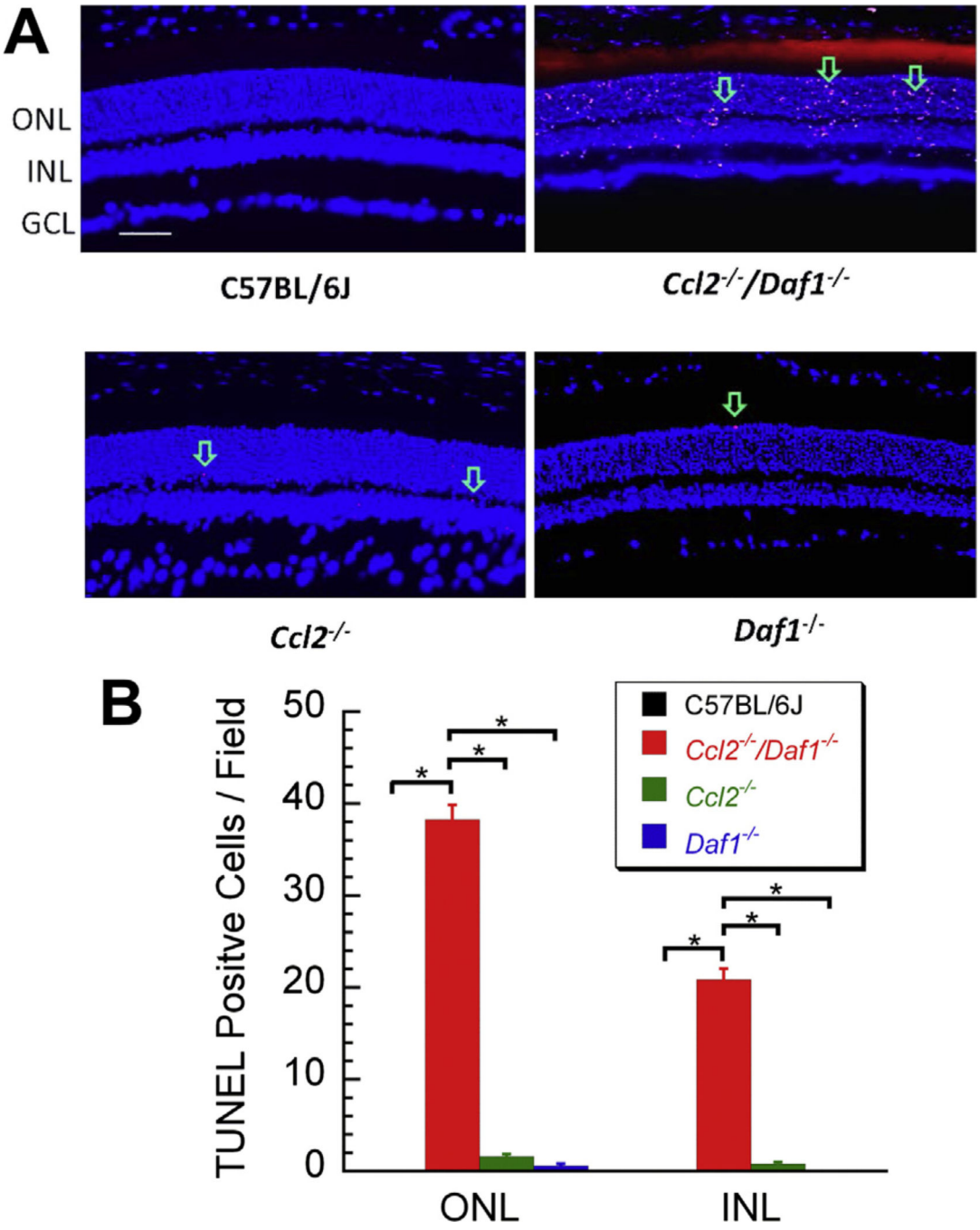

Fig. 4.

TUNEL analysis. (**A**) Representative images of retinal sections taken next to the optic nerve head for each genotype. The arrows indicate some of the TUNEL-positive cells which are seen in the ONL and the INL of mutant but not C57BL/6J mice. The scale bar indicates 50 μm. (**B**) Average number of TUNEL-positive cells counted in the ONL (left) and INL (right) of C57BL/6J, *Ccl2*$^{-/-}$/*Daf1*$^{-/-}$, *Ccl2*$^{-/-}$, or *Daf1*$^{-/-}$ mice. The greatest number was noted in *Ccl2*$^{-/-}$/*Daf1*$^{-/-}$ retinas. Bars indicate the mean ± SE for three mice of each genotype. *$p <$ 0.01.

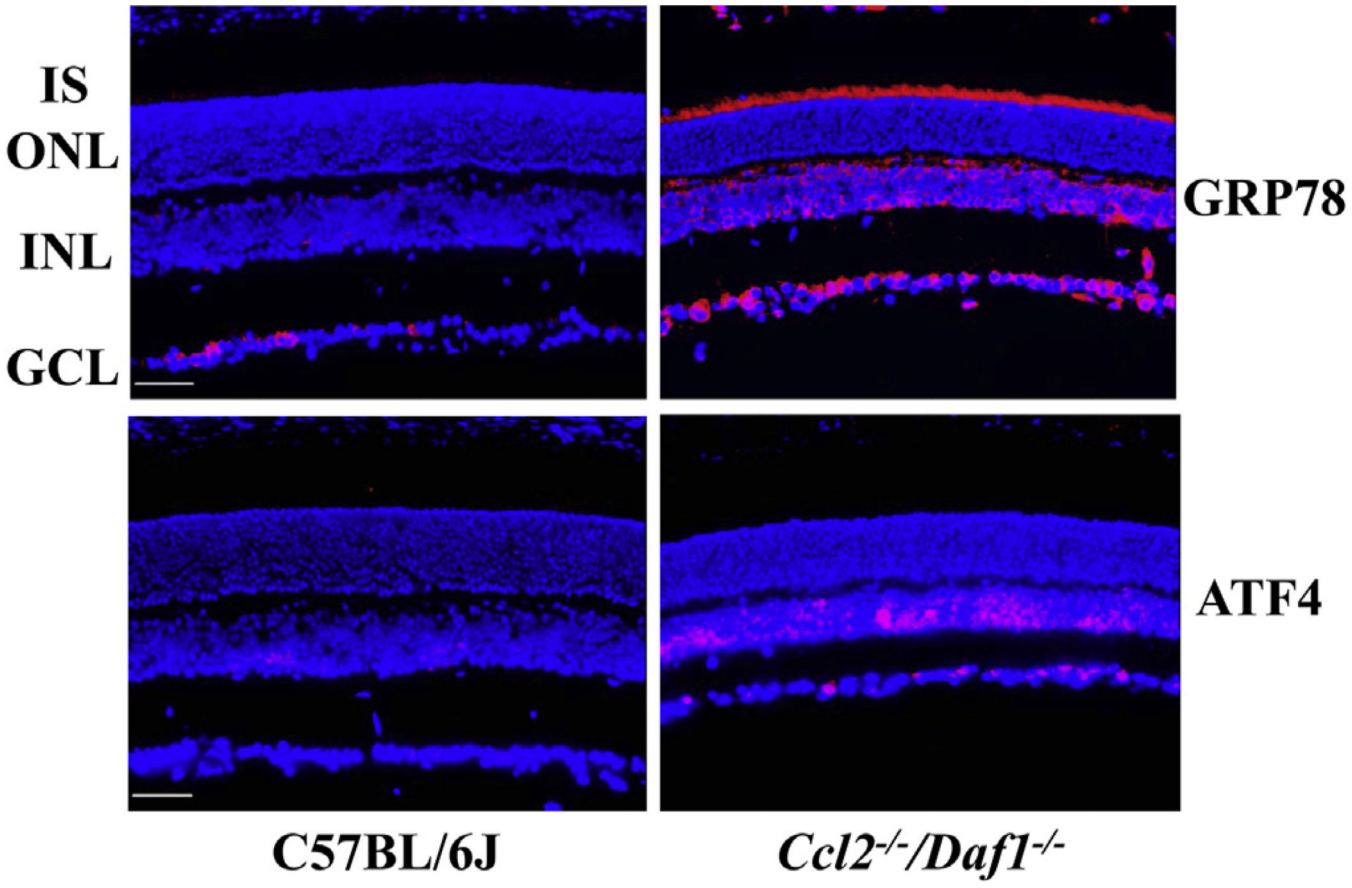

Fig. 5.

Immunohistochemical analysis of ER stress marker distribution in C57BL/6J and *Ccl2*$^{-/-}$/*Daf1*$^{-/-}$ mice. Staining for GPR78 and ATF4 is significantly increased in the *Ccl2*$^{-/-}$/*Daf1*$^{-/-}$ retina. The scale bar indicates 50 μm. Images are representative of 3 mice per genotype.

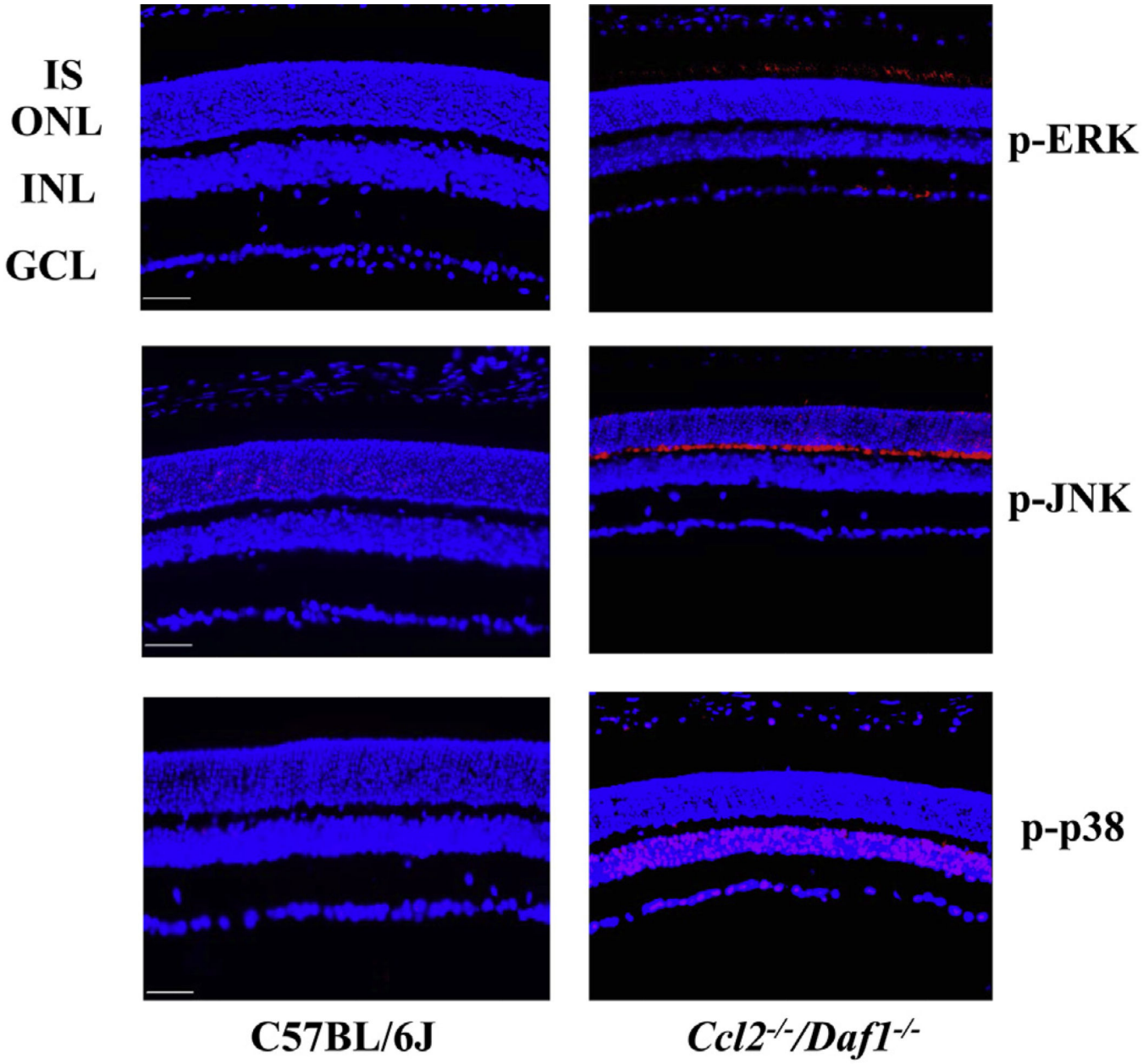

Fig. 6.

Immunohistochemical analysis of p-ERK, p-JNK and p-p38 distribution in C57BL/6J and *Ccl2*$^{-/-}$/*Daf1*$^{-/-}$ retina. Staining for p-ERK, p-JNK and p-p38 is significantly increased in the *Ccl2*$^{-/-}$/*Daf1*$^{-/-}$ retina. The scale bar indicates 50 μm. Images are representative of 3 mice per genotype.

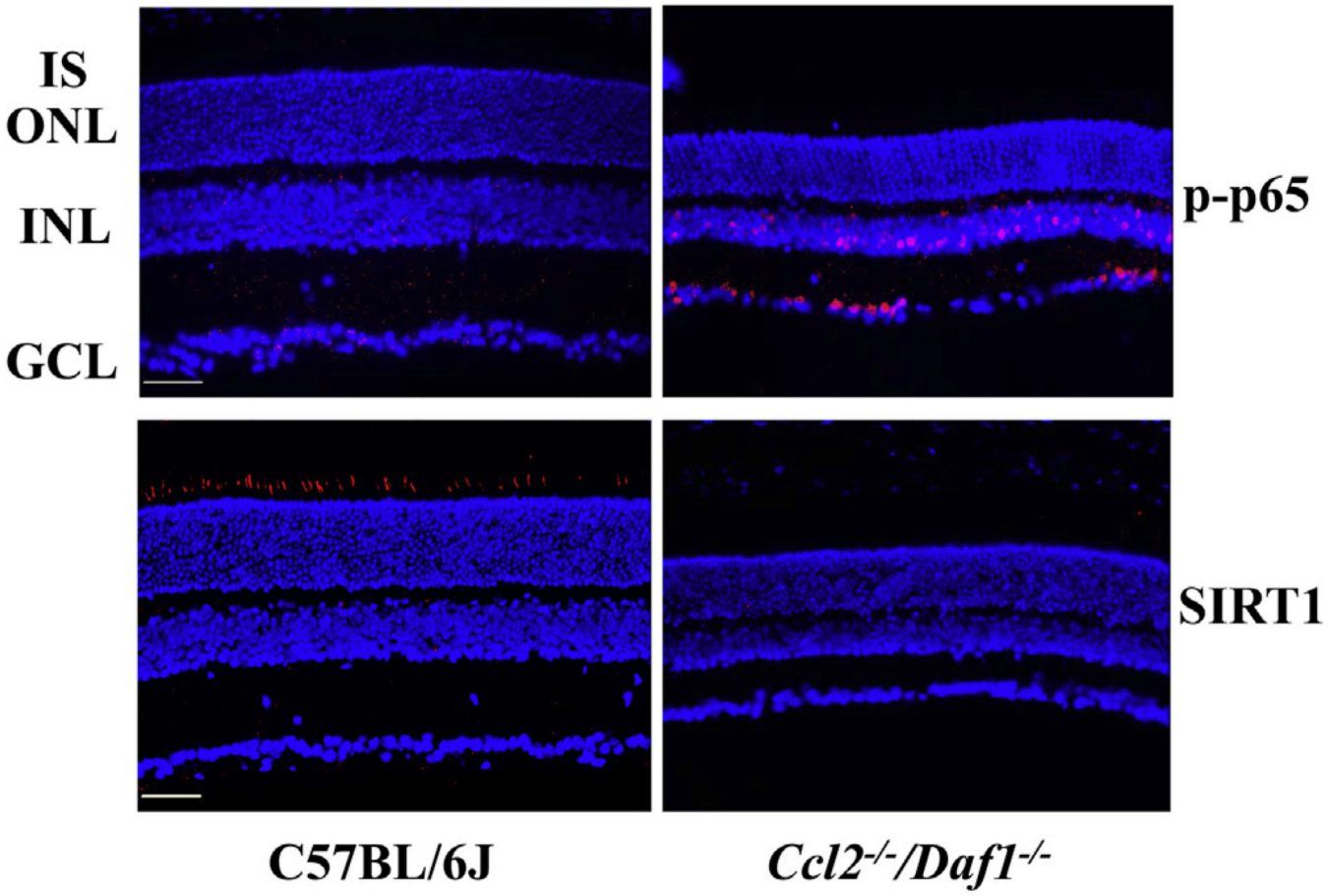

Fig. 7.

Immunohistochemical analysis of p-p65 and SIRT1 distribution in C57BL/6J and *Ccl2*$^{-/-}$/*Daf1*$^{-/-}$ retina. The scale bar indicates 50 μm. Images are representative of 3 mice per genotype.